Article No. mb981940 *J. Mol. Biol.* (1998) **281**, 501–511

JMB

A Structural Basis for Transition-state Stabilization in Antibody-catalyzed Hydrolysis: Crystal Structures of an Abzyme at 1.8 Å Resolution

Ole Kristensen, Dmitry G. Vassylyev, Fujie Tanaka, Kosuke Morikawa* and Ikuo Fujii*

Biomolecular Engineering Research Institute, and Protein Engineering Research Institute 6-2-3 Furuedai, Suita Osaka 565, Japan

The three-dimensional structure of a catalytic antibody, 6D9, has been solved as a complex with a transition state analog. The structure was determined from two different crystal forms, and was refined at a resolution of 1.8 Å. The antibody 6D9, which was induced by immunization with the phosphonate transition state analog **3**, hydrolyzes a prodrug of chloramphenicol monoester **1** to generate the parent drug **2**. The kinetic studies have shown that the antibody is catalytic by virtue of the theoretical relationship between the affinity for the transition state and the catalytic efficiency ($k_{cat}/k_{uncat} = K_S/K_{TSA}$). The crystal structure makes it possible to visualize the theoretical relationship. A side-chain (N^{ε}) of His^{L27D} is placed in a key position to make a hydrogen bond to the phosphonate oxygen of the transition state analog with a distance of 2.72 Å, suggesting a hydrogen bond to the oxyanion developing in the transition state of the hydrolysis. There are no catalytic residues, other than the histidine, around the phosphonate moiety. In addition, in the antibody-hapten complex, the hapten bears a folded conformation and the two stacked aromatic rings are buried deep in the antigen-combining site through aromatic-aromatic interaction with Trp^{H100I} and Tyr^{H58}. The conformation of the bound hapten suggests that the antibody binds the substrate to change the conformation of the ester moiety to a thermodynamically unstable *E*-form, thereby making it easy for the substrate to reach the transition-state during catalysis. These observations reveal that the catalytic mechanism is explained purely on the basis of the stabilization of the transition state. The refined high resolution structures reported here are envisaged to have an impact on the understanding of other hydrolytic antibodies, since their haptens share some unique features with the hapten used in this study.

Keywords: catalytic antibody; X-ray crystallography; Fab; transition-state stabilization

**Corresponding authors*

Introduction

Since the mammalian immune system is characterized by an almost limitless potential for providing receptor-like molecules for virtually any chemical structure, catalytic antibodies can provide the tailor-made catalysts for reactions, in which no natural counterpart exists (Schultz & Lerner, 1995; Lerner & Schultz, 1993; Lerner *et al.*, 1991; Shokat & Schultz, 1990; Tramontano *et al.*, 1986). Such antibodies have been generated against the putative transition state analogs (TSA), with the expec-

Present addresses: O. Kristensen, Department of Molecular Biophysics, Chemical Center, Lund University, Getingevägen 60, 221 00 Lund, Sweden; D. G. Vassylyev, International Institute for Advanced Research, Matsushita Electric Industrial Co., Ltd, 3-4 Hikaridai, Seika, Soraku, Kyoto 619-02, Japan.

Abbreviations used: TSA, transition state analog; CDR, complementarity determining region.

E-mail address of the corresponding author: fujii@beri.co.jp

0022–2836/98/330501–11 $30.00/0

tation that the induced antigen-combining site could be both geometrically and electronically complementary to the transition state for the reactions, and might stabilize this species through a variety of enthalpic or entropic contributions. Therefore, for catalytic antibody research, it is important to understand the relationship between the chemical properties of the TSAs and the catalytic functions of the induced antibodies. The theoretical relationship has been evaluated by correlating the catalytic activity of an antibody and the differential binding of the TSA and the substrate (Fujii *et al.*, 1995; Stewart & Benkovic, 1995). If antibodies are catalytic by virtue of the theoretical relationship between the affinity for the transition state and the catalytic efficiency, the ratio of the dissociation constants for the transition state analog (K_{TSA}) and the corresponding substrate (K_S) should be equal to the rate enhancement ($k_{cat}/k_{uncat} = K_S/K_{TSA}$). To visualize this concept, here, we have determined the crystal structures of the Fab fragment of antibody 6D9 in complex with a transition state analog.

Catalytic antibody 6D9, which was induced by immunization with the haptenic phosphonate **3**, catalyzes the hydrolysis of a non-bioactive chloramphenicol monoester derivative **1** to generate chloramphenicol **2**, as shown in Figure 1 (Miyashita *et al.*, 1993). Among the large number of hydrolytic catalytic antibodies, of which a few have been examined to define the three-dimensional structures by X-ray crystallography (Wedemayer *et al.*, 1997; Charbonnier *et al.*, 1995, 1997; Patten *et al.*, 1996; Zhou *et. al.*, 1994), catalytic antibody 6D9 is characterized as an antibody that functions strictly according to the theoretical relationship described above. Thus, the rate enhancement ($k_{cat}/k_{uncat} = 895$) observed with 6D9 is in close agreement with the ratio ($K_S/K_{TSA} = 900$) of the binding affinities to the transition-state analog and the substrate. This suggests a reaction mechanism in which the antibody-hapten binding interactions are also present in the transition-state and serve to accelerate the reaction rate. Thus, the antibody 6D9 should provide a suitable system to analyze the correlation among transition state analogs, active site structures, and catalytic functions. In addition, the extensive data characterizing the catalytic activity of 6D9, obtained by kinetic, mutation, and chemical modification studies can be used to discuss the catalytic structure (Miyashita *et al.*, 1997; Fujii *et al.*, 1995).

Here, we report crystal structures of the Fab 6D9 complexed with a phosphonate derivative **4**. Although we attempted to crystallize the Fab fragment as a complex with both the original hapten **3** and its derivatve **4**, only the complex with **4** enabled us to determine the crystal structure at high resolution: The additional atoms incorporated into derivative **4** seem to fill a void in the crystal lattice to beneficially affect the crystal packing. Our results showed that the structual modification, introduced at the phosphonate moiety, extends as an appendage into the solvent region, and thus is not involved in the antibody-ligand binding interaction. This is supported by an evidence that the derivative **4** displayed a dissociation constant (K_d) and an inhibition constant (K_i) practically identical to those of immunized hapten **3**. Thus, these observations allowed us to discuss the mechanistic

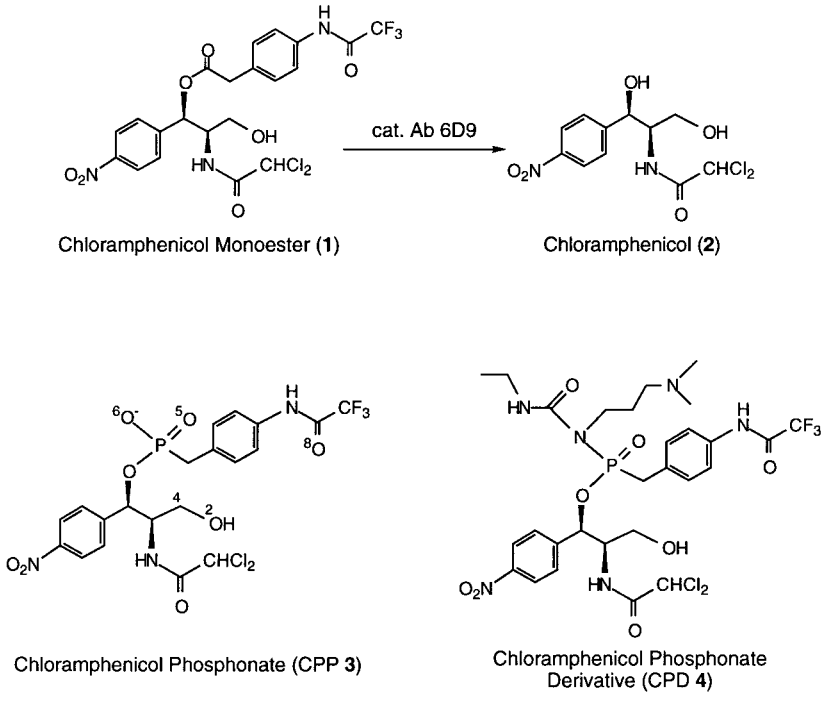

Figure 1. Chemical transformation in the model system for the antibody 6D9 catalyzed prodrug activation. For immunization, the hapten **3** was coupled to the carrier protein at the position of oxygen O^2. In the crystals, the hapten **4** is bound to the active site.

interpretation of the antibody-catalyzed reaction in relation to the X-ray structures. The crystal structures of the Fab 6D9 with a putative transition state analog bound at the active site, reported here, provide a detailed description of the combining site environment, and lend support to a simple catalytic mechanism, involving only the attributes of transition state stabilization.

Results

Quality of the structures

The two crystal structures of the Fab 6D9 transition state complex superimpose with r.m.s. differences of 0.29 Å and 0.57 Å for the variable and constant domains, respectively, including all C^{α} coordinates in calculations with the program LSQMAN (Kleywegt & Jones, 1994), and show overall similarity to other known antibody structures (Figure 2). The atomic positions of the haptens in the two models are very similar, with an r.m.s. deviation of 0.90 Å, including all atoms. The six variable domain loop regions, containing the heavy (H1 to H3) and light (L1 to L3) chain CDR sequences, are found at the N-terminal tip of the molecule (Figure 3). The Fab 6D9 molecule is almost straight, with an elbow angle of close to 176° in both models.

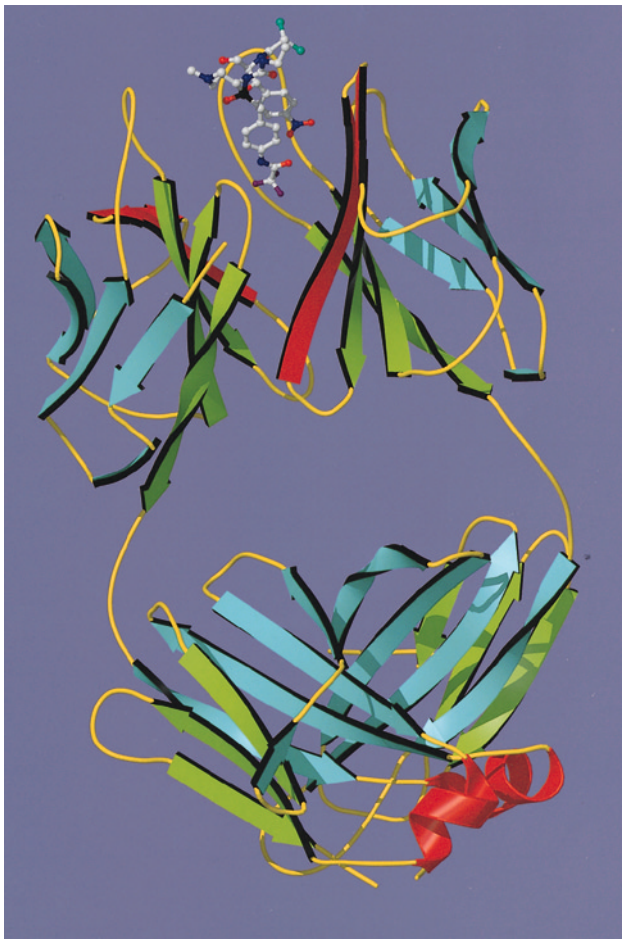

Figure 2. Cartoon of the overall Fab 6D9 structure. Although similar to other known immunoglobulins, some details of the β-strand associations differ from the standard textbook image (Branden & Tooze, 1991). Furthermore, it should be noted that the structure contains well-defined helical segments. The CPD hapten is shown at the tip of the molecule.

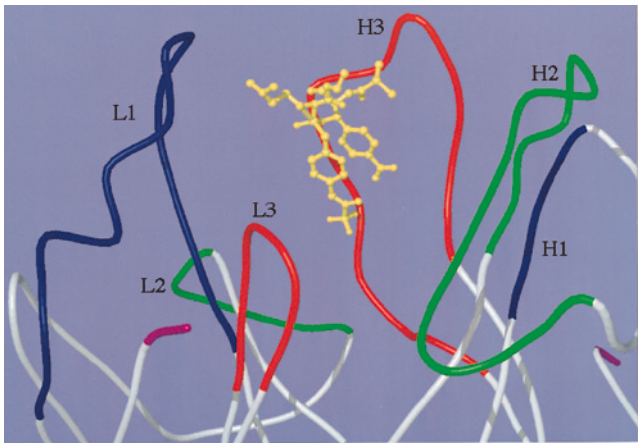

Figure 3. Sketch showing the position of the hapten close to the prominent CDR H3.

The electron density for the constant domain loop region, ranging from H128 to H134, is notably poor in the otherwise high quality maps. This results in small real space correlation coefficients in the corresponding region between the two crystal structures (Figure 4). The poor density and the high thermal parameters of these surface residues have been noted in other studies (Arevalo *et al.*, 1994; Golinelli-Pimpaneau *et al.*, 1994; Stanfield *et al.*, 1990; Tulip *et al.*, 1992). An analysis with the program PROCHECK (Laskowski *et al.*, 1993) revealed that the overall stereochemical quality of the model from form I was similar to that of other protein structures solved at the same resolution. The main-chain geometries of 86.5 of the residues occupied the ''most favored'' regions in the Ramachandran plot. One of the three peptide units (Val^{L51}) with ''disallowed'' values for the ϕ, ψ angles has been seen to assume a non-standard conformation in other structures (Arevalo *et al.*, 1994). In addition, the hydrogen bond energies, the bad contacts in terms of non-bonded interactions, and the side-chain geometries were either better than or close to the average obtained from other structure determinations.

The structural quality of the model from form II, as judged by the PROCHECK routines, was marginally better than the model derived from the form I crystal. The electron density and the temperature factor distribution confirmed the high flexibility or disorder of the constant domain region, H128 to H134, but in general, the refined model allows the detailed

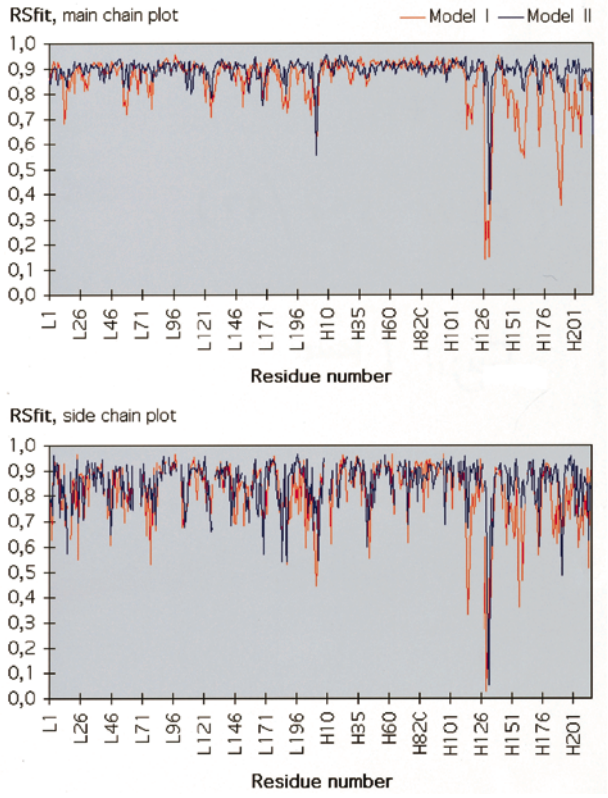

Figure 4. Plots of the real space correlation coefficient *versus* the sequence position for the main-chain (upper) and side-chain atoms (lower). The data reveal that the heavy chain region H128 to H134 is disordered in both models of the Fab 6D9-CPD complex.

and clear structural descriptions (Figure 5). Additional data for both models are summarized in Table 1.

The binding pocket

The hapten binds with high complementarity to an indentation in the surface of the antigen combining site, as often found in antibodies binding haptens of similar size (Padlan, 1994; Figure 6). The cavity has the character of a pocket, rather than a long groove which would be expected if the transition state analog bound in an extended conformation. Thus, the folded binding mode of the hapten, which allows stacking interactions between the two aromatic rings of the hapten molecule, is congruent with the shape of the binding site. A comparison with *B*-DNA revealed that the approximate distance of 4.0 Å between these aromatic components, in addition to their precise geometric arrangement, is at least as favorable for such interactions as in the case of DNA nucleotide bases. The hapten is oriented with the stacked aromatic rings at the center of the pocket, the trifluoroacetyl portion at the bottom, and the tetrahedral phosphonate moiety exposed towards the solvent. The *N*-(2-hydroxyethyl)dichloroacetamide portion of the hapten is close to the surrounding water at the tip of the combining site. For immunization, the hapten **3** was coupled *via* a linker to the carrier protein through the oxygen O^2, which lies at the cleft entrance, thereby indicating that the hapten molecule itself served as the primary epitope.

The antigen-antibody interactions

The antibody 6D9 generates energy for hapten recognition through a combination of hydrophobic, electrostatic, and hydrogen-bonding interactions. The two stacked aromatic rings of the hapten form the center of a hydrophobic core in the liganded combining site (Figure 7). These aromatic rings appear to be associated with Trp^{H100I} and Tyr^{H58}, presumably through aromatic-aromatic interaction, as revealed from the orientation of the hapten aromtaic rings perpendicular to the two aromatic side chains of the antibody (Burley & Petsko, 1985). In addition to the perpendicular aromatic interactions, a π-stacking interaction between His^{H97} and the *p*-nitrophenyl group of the hapten was observed. Thus, the aromatic interaction among the five aromatic rings appears to be important for the hapten binding. Furthermore, the side-chains of Phe^{L89}, Phe^{L98}, Phe^{H100K}, and Val^{H95} form a hydrophobic environment at the bottom of the binding pocket. In this region, the haptenic nitro group appears to contact the protein only by van der Waals interactions, and not through hydrogen bonding.

The light chain CDR2, which is outside the combining site, and the heavy chain CDR1 loops provide no residues contributing to the antigen-antibody interaction. In contrast, residues from the remaining four CDRs are involved in binding pocket formation. The light chain CDR1 has three residues facing the catalytic cavity: Ser^{L27E}, Asn^{L28}, and the important His^{L27D}. The light chain CDR 3 includes two residues, Phe^{L89} and Gly^{L91}, playing important roles in the hapten recognition. A significant dipole-induced interaction exists between the carbon-fluorine bond of the hapten and the side-chain of Phe^{L89}, which is at a distance of less than 4.0 Å. from the halogen atom. The main-chain carbonyl oxygen of Gly^{L91} and the side-chain of Trp^{H100I} form the hydrogen bond, which is important to fix the position of H3. The heavy-chain CDR H2 provides Ser^{H50}, which participates in a hydrogen bond to the oxygen O^8 of the bound hapten, and Tyr^{H58}, which is a component of the hapten-centered aromatic-aromatic interaction. The heavy chain CDR3 loop embraces the transition state analog and is essential to define the antigen binding pocket. The main-chain nitrogen atom of Gly^{H100} and the N^{ε} atom of His^{H97} are involved in hydrogen bonding to the carbonyl group of the dichloroacetamide group.

The distribution of ordered solvent molecules around the Fab molecule follows the pattern generally observed in other proteins. Interestingly, no

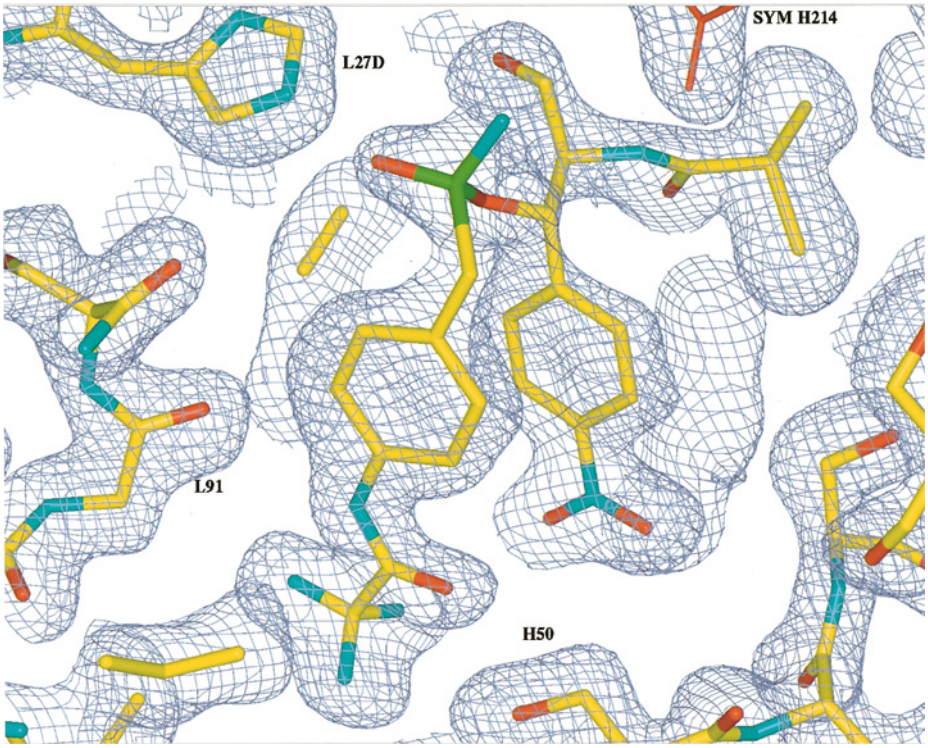

Figure 5. View of the $2F_o - F_c$ electron density map (contoured at a 1.0σ level) in the hapten binding region. The map was calculated based on the data obtained from form I crystal and the refined model. In a different orientation, the density shows clear invaginations at the center of the aromatic functionalities of the hapten, illustrating that its position is defined accurately.

internal hydration was observed around the bound transition state analog in the active site of 6D9; water molecules seem to be excluded rather than included in the hapten binding, in contrast to the situation recently reported for anti-sweetener Fab complex (Guddat *et al.*, 1994).

The dissociation and inhibition constants for the haptenic phosphonates, 3 and 4

In the present crystallographic study, the compound **4** was bound to the active site of the antibody 6D9. Although the compound **4** is a derivative of the original hapten **3**, the complex of the Fab 6D9 with **4** allowed us to determine the crystal structure at high resolution. Our structural results show that the structural modification introduced at the phosphonate moiety of the hapten extends as an appendage into the solvent region, and that it is not involved in antibody-ligand binding interactions (Figures 6 and 7 (upper)). To support this observation, we have examined the binding affinity of the haptens **3** and **4** and the inhibition patterns during the catalysis, since other studies of antibody-ligand complexes have shown that even small structural alterations in the binding pattern can seriously affect the binding affinity (Chacko *et al.*, 1995). Dissociation constants for the binding of the two haptens **3** and **4** to the Fab 6D9 have been determined by fluorescence titration,

Table 1. Data collection (Kristensen *et al.*, 1995) and refinement statistics

Crystal form:	I	II
Space group:	$P2_1$	$P2_1$
Cell dimensions:	$a = 55.91$, $b = 61.66$, $c = 66.67$ Å, $\beta = 104.68°$	(form I)
	$a = 58.70$, $b = 63.04$, $c = 56.56$ Å, $\beta = 98.75°$	(form II)
Resolution limit applied (Å):	6.0–1.8	6.0–1.8
No. unique reflections:	27,402	32,963
No. non-hydrogen atoms:		
Protein[a]:	3369	3360
Hapten:	48	48
Solvent:	140	217
R^b_{cryst} (%):	19.8	22.8
R^c_{free} (%):	28.2	29.5
r.m.s. deviations in:		
Bond length (Å):	0.007	0.008
Bond angles (°):	1.382	1.492
Dihedrals (°):	30.10	30.18
Impropers (°):	0.707	0.739

[a] In form II, the disordered region H131 to H133 was left as alanine residues.

[b] $R_{cryst} = \Sigma|F_o - F_c|/\Sigma F_o$, where F_o and F_c are observed and calculated amplitudes, respectively, of structure factors for reflections used in the refinement.

[c] A random set of reflections, representing ten (form I) and five (form II) % of the initial data, was excluded from the model refinement. All data were measured with an average six to sevenfold redundancy, which is normally not achieved in monoclinic space groups.

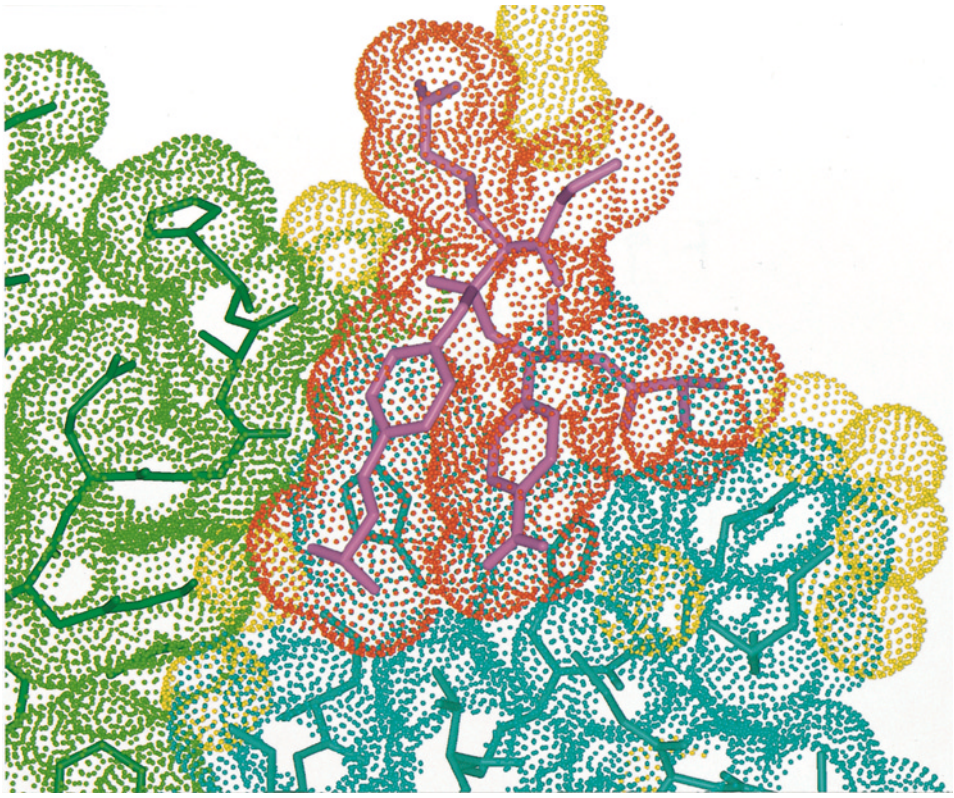

Figure 6. The van der Waals molecular surfaces are found to be highly complementary between the antibody 6D9 combining site (green and cyan) and the hapten (red). Water molecules are shown in yellow. The program XtalView (McRee, 1992) was used to generate the surfaces and provided an interface to render the Figure with Raster3D (Meritt & Murphy, 1994).

which provided K_d values of 13(±6) and 19(±2) nM, respectively. The practically identical K_d values suggest that the alteration between **3** and **4** does not effect the binding affinity in the 6D9-ligand interaction. In addition, both haptens showed similar inhibition patterns during the antibody-catalyzed hydrolysis. An analysis with the Dixon plots displayed competitive inhibition, providing K_i values of 60(±6) and 50(±9) nM for haptens **3** and **4**, respectively. Thus, it is anticipated that the presence of the substituent at the oxygen position O^5 will have no effect on our mechanistic interpretation.

Discussion

Structural studies of hydrolytic catalytic antibodies have revealed antigen-combining sites, in which a couple of catalytic functions work in concert (Wedemayer *et al.*, 1997; Charbonnier *et al.*, 1995, 1997; Patten *et al.*, 1996). For example, antibody 17E8 catalyzes the hydrolysis by a concerted mechanism of transition-state stabilization with a Lys and nucleophilic catalysis with a Ser-His dyad in the antigen-combining site, as revealed from the X-ray crystal structure (Zhou *et al.*, 1994) and kinetic studies (Guo *et al.*, 1994). This proposal seems to be consistent with the transition state analysis of 17E8, in which the rate acceleration factor ($k_{cat}/k_{uncat} = 8900$) deviated from the affinity ratio ($K_m/K_i = 430$). Our structural studies of 6D9 also identified an important histidine involved in transition state stabilization in the antigen-combining site. However, there are no catalytic residues, other than the histidine, around the phosphonate moiety of the hapten, as evidenced with the transition state analysis ($k_{cat}/k_{uncat} = 895$, $K_S/K_{TSA} = 900$). Consequently, the structural data, together with the previous kinetic study, facilitate simple discussions of the structural basis of transition state stabilization in antibody catalysis.

As shown in the X-ray structure of 6D9 (Figure 7), a side-chain (N^{ε}) of His^{L27D} is placed in a key position to make a hydrogen bond to the phosphonate oxygen of the transition state analog with a distance of 2.72 Å. With the exception of His^{L27D}, a tyrosine, Tyr^{H58}, appears to be relatively near the phosphonate of the hapten. However, the hydroxyl group would be too remote to serve as a catalytic residue for a nucleophilic attack, even with the proviso of side-chain movement, in addition, there are no residues which activate the hydroxyl group. Thus, no protein functional group appears to be appropriately placed to act as a potent nucleophile. Given the lack of a nucleophile in the active site, water or hydroxide ions are the obvious choice to attack the substrate. Consequently, these observations lend support to the idea that the catalytic activity is mediated through transition state stabilization, by hydrogen bonding

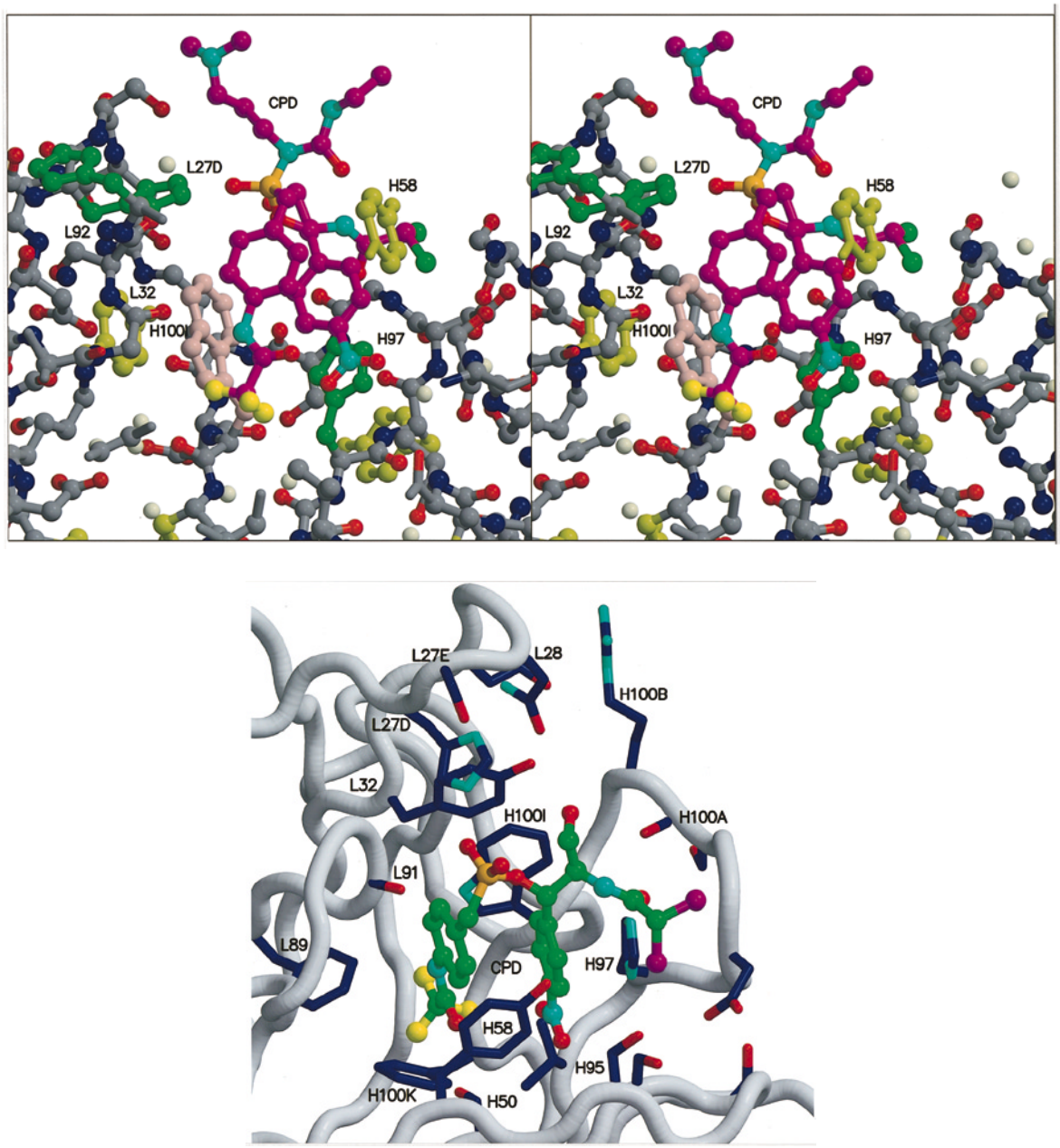

Figure 7. Close-up of the active site of the catalytic antibody 6D9. The atomic coordinates are based on the form I data. Water molecules (light yellow) seem to be excluded from the combining site upon ligand binding, and the appendage of the CPD hapten extends into the solvent region (upper). A simplified representation, which shows only some selected side-chains, provides an alternative view of the binding pocket (lower). For clarity, the hapten is represented as the transition-state analog CPP.

of the histidine side-chain to the tethrahedral transition state. The structual data are well consistent with the mutagenesis (Miyashita *et al.*, 1997). Mutation of Tyr^{H58} to phenylalanine did not essentially affect the hydrolytic activity as compared to that of the native 6D9, while the alanine mutant of His^{L27D} lost the activity completely. On the other hand, an alternative possibility for the role of the histidine is to act as a nucleophilic or general-base catalyst. This has been proposed by Lerner and coworkers in their study of the esterolytic antibody (6D4), which also possessed a crucial histidine residue, that participated in either nucleophilic or general base catalysis, with the prevailing pathway determined by the choice of substrates (Tramontano *et al.*, 1986). However, the kinetic studies of antibody 6D9 rule out the possibility of the histidine functioning as a nucleophilic or general-base catalyst; the antibody-catalyzed hydrolysis proceeds with a first-order dependence on hydroxide ions (log k_{cat} plotted against pH) and without either burst kinetics or noticeable reaction inhibition (Fujii *et al.*, 1995).

Theoretical and crystallographic studies of thermolysin in complex with various inhibitors have provided an estimate of 4.0 kilocalories per mole

for the intrinsic binding energy contained in the specific hydrogen binding interaction between an amide NH and a charged oxygen of a phosphoamidate transition state inhibitor (Bartlett & Marlowe, 1987; Bash *et al.*, 1987; Tronrud *et al.*, 1987). In 6D9, the difference ($\Delta\Delta G$) in free energy between the antibody-catalyzed and uncatalyzed (background) reactions and the difference ($\Delta\Delta G$) in the binding energy between the transition state and the ground state were calculated, based on the values of k_{cat}/k_{uncat} and K_S/K_{TSA}, respectively, to be 4.0 kilocalories per mole for both (Fujii, *et al.*, 1995). From the X-ray structure, the side-chain of His^{L27D} was found to play an important role for stabilization of the tetrahedral transition state. However, the hydrogen bond of His^{L27D} to the tetrahedral transition state may not be sufficient to account for the catalytic properties of this immunoglobulin catalyst. Since His^{L27D} is at the tip of the antigen-combining site, a binding energy of the hydrogen bond is likely to be less than 4.0 kilocalories per mole. In addition to His^{L27D}, the aromatic-aromatic interaction with Trp^{H100I} and Tyr^{H58} also contributes to the transition-state stabilization. In the antibody-hapten complex, the hapten bears a folded comformation and the two stacked aromatic rings are buried deep in the antigen-combining site through the aromatic-aromatic interaction. The conformation of the bound hapten suggests that the antibody binds the substrate to change the conformation of the ester moiety to the thermodynamically unstable *E*-form, thereby making it easy for the substrate to reach the transition-state during catalysis: It is well known that esters are planar and that the *E*-form is much more unstable than the *Z*-form (Deslongchamps, 1983). The conformational change of the ester moiety from a stable *Z*-form to an unstable *E*-form leads to a weak substrate binding affinity of the antibody. The transition-state stabilization observed in 6D9-catalyzed hydrolysis is likely due to a pertubation between the intrinsic binding energy to the transition state and the weak binding to the substate (Fersht, 1985). These observations reveal that the catalytic mechanism is explained purely on the basis of the stabilization of the transition state.

The structural reasons for the substrate specificity of the antibody 6D9 can readily be understood from the detailed image of the combining site obtained from the structure determinations. Replacement of the nitro group with a dichloroacetamido substituent resulted in a substrate that was not processed by 6D9. The crystal structure shows that this modification cannot be accommodated, due to steric conflict with the binding pocket. Changes of the appendage at C^4 of the substrate can be tolerated, in agreement with the solvent exposed position seen in the crystal structures. As mentioned above, an interesting outcome of this structural study is the discovery of the folded hapten conformation and the binding of both the *N*-trifluoroacetylaminophenyl and *p*-nitrophenyl groups in the hydrophobic environment at the bottom of the active site cavity. A previously reported molecular modeling successfully predicted the antigen-combing site structure, but not the bound-hapten conformation, which was assumed to be extended, rather than compactly folded (Fujii *et al.*, 1995). The fact that the two stacked benzene rings are entirely buried in the antigen-combining cavity, and neither the fluorine atoms nor the nitro group is hydrogen bonded, provides a rationale as to why the 6D9 catalyst is not severely limited by product inhibition. Thus, the folded state of the two benzene rings is the important epitope. Each product of the mono benzene derivative would no longer possess sufficient binding affinity to cause product inhibition.

Recently, structural models of hydrolytic antibodies, which were independently derived from different mice and different haptens, have been reviewed. It was noted that a common structural motif was induced to achieve a catalytic advantage when the immune system was stimulated by immunization with antigens containing aryl phosphonate groups (MacBeath & Hilvert, 1996). In contrast to their proposal, the antibody 6D9 shows a different catalytic structure of the antigen-combining site, despite the fact that the antibody was also elicited against an aryl phosphonate antigen. As compared with the other antibodies, 6D9 possesses a light chain CDR1 (16 amino acids) and a heavy chain CDR3 (14 amino acids) with longer amino acid sequences (Miyashita *et al.*, 1994), which result in an antigen-combining site with a cavity opened relatively wide; for example, CNJ 206 possesses the LCDR1 of 11 amino acids and the HCDR3 of 10 amino acids. The antigen binding of 6D9 is dominated by amino acid residues within the extended loop structures of the two CDRs. Especially, in comparison with the other hydrolytic antibodies, the structure of the antigen-combining site is characterized by the potential to bind the two stacked aromatic rings of the ligand, which additionally contributes to the transition-state stabilization as mentioned above. Since the hapten used in this study shares some of the unique features of other haptens used for catalytic antibodies, the refined high resolution structures reported here are envisaged to have an impact on the understanding of other hydrolytic antibodies. Furthermore, the structural information is useful for understanding a single process of transition-state stabilization in enzyme catalysis on a structural basis, as well as for increasing catalytic efficiency by site-directed mutagenesis and for designing a new hapten that induces catalytic antibodies with higher activity.

Materials and Methods

Data collection

The two different crystal forms of the 6D9 Fab fragment complexed with a transition state analog have been characterized in this study. The details of crystallization

and the data collection have been described (Kristensen *et al.*, 1995).

X-ray diffraction data were collected from two form I crystals, using both a conventional X-ray source (a MacScience M18X rotaing anode generator equipped with a DIP100 imaging plate system) and synchrotron radiation (beam line BL6A2, Photon Factory, Tsukuba). The WEIS data processing software packages were used to integrate the intensities (Higashi, 1989). The data were merged and scaled by means of the program PROTEIN (Steigemann, 1974). Diffraction data from two form II crystals were recorded exclusively using synchrotron radiation and the Weissenberg camera installed at the Photon Factory. The data were processed by the programs DENZO and SCALEPACK (Otwinowski, 1993).

Structure determination and refinement

The peptide binding antibody B13I2 (Stanfield *et al.*, 1990), which specifically binds a synthetic homolog of the C-helix of myohemerythrin, was used as a search model in the molecular replacement solution of the Fab 6D9-hapten complex. Both antibodies, 6D9 and B13I2, belong to the same isotypic subgroup (IgG1, kappa light chain), and the overall sequence identity is 92.4%.

The structure determination was first carried out based on the form I data. Since the crystals contained only one Fab molecule in the asymmetric unit, it was anticipated that an intact Fab model (four domains) would provide a reasonable starting point for the calculations. The peptide antigen, as well as the *N*-acetyl-D-glucosamine modification of an asparagine residue, was omitted from the coordinate file deposited in the Brookhaven Protein Data Bank (entry-code: 2igf). At this stage, no attempts were made to correct for the differences in the sequences of the two antibodies. The program package X-PLOR was used for the molecular replacement (MR) calculations, as well as for the refinement (Brünger, 1992).

Rotation functions evaluated data between 8.0 and 3.5 Å and restricted model Patterson vectors (4 to 24 Å in length) yielded a cross-rotation map with enough features to recognize the correct solution. The orientations of the model, indicated by the list of peaks, were optimized and tested by adjustment of the relative positions of the four Fab domains (V_L, V_H, C_L, and C_H1) by the rigid body refinement procedure. The top three peaks represented practically the same orientation. However, only the third peak was sufficiently precise to permit a stable refinement. The validity of this orientation was confirmed by Patterson correlation refinement (Brünger, 1990), which provided the Euler angles θ_1, θ_2, $\theta_3 = (25.302,\ 74.000,\ 28.635)$ to be applied for the rotational component. With the 8.0 to 3.5 Å resolution data, a search revealed the correct position of the model to be indicated by the single strong peak in the translation function, which in fractional coordinates was determined as $x,\ y,\ z = (0.463,\ 0.0,\ 0.160)$. The four domains of this positioned model were then allowed to move as independent units in rigid body refinement. The crystallographic *R* value at this stage was 41.5% for data between 6.0 and 3.0 Å. The $2F_o - F_c$ map, calculated after conjugate gradient minimization and refinement of the model by simulated annealing (SA) using the slow-cooling protocol, showed clear electron density for the major part of the molecule. From a global viewpoint, the complementarity determining regions of the variable domain were definable, except for the H3 loop. Although relatively abundant, the electron density in this region was unconnected. Using the ''mutate option'' in the program O (Jones *et al.*, 1991), the non-cognate residues of the model were changed to fit the sequence of the Fab 6D9, and the necessary insertions and deletions were introduced. Multiple cycles of X-PLOR refinement (Powell minimization and SA), combined with rebuilding of the model with O, did not significantly improve the density for the important CDR H3 region. The calculation of the $F_o - F_c$ omit maps provided insufficient information to facilitate real progress. After unrestrained refinement of the grouped temperature factors (*B*-factors), the crystallographic *R* value came to rest at 24% for the data between 6.0 and 2.0 Å. An electron density map, calculated based on a solvent flattening procedure with restrained phases (Wang, 1985), improved the situation dramatically and made it a tangible task to trace the H3 loop. The density for the hapten in the antibody-combining site was clearly seen to reside in the vicinity of the prominent CDR H3. After several cycles of refinement, including manual adjustment, SA at 4000 K, and restrained individual *B* factors, 140 water molecules were sequentially added to the model, using the CCP4 program WATERPEAKS (SERC, 1979) and the ''pekpik option'' in O. The final *R* value is 19.8 % for the data between 6.0 and 1.8 Å. A decreasing free *R* value confirmed the progress of the model (Brünger, 1990). The final model agrees with the data (6.0 to 1.8 Å) to produce a free *R* value of 28.2 %.

The structure of the Fab 6D9 transition state complex, as crystallized in the second crystal form, form II, was solved generally as described above, with the use of the refined coordinates of the form I model. One cycle of refinement with the X-PLOR simulated annealing protocol resulted in an *R* value of 26.4 % for the 6.0 to 2.5 Å data. The refined structure includes 217 water molecules and represents a model with an *R* value of 22.8 % for data between 6.0 and 1.8 Å. The free *R* value is 29.5%.

The approximately 2-fold related units of the Fab (V_L/V_H and C_L/C_H) were superimposed to optimize the fit using the program LSQMAN (Kleywegt & Jones, 1994). The following residues were used: V_L: 1 to 23, 35 to 48, 61 to 87, and 98 to 107; V_H: 1 to 22, 36 to 49, 66 to 91, and 103 to 112; C_L: 109 to 117, 129 to 142, 144 to 149, 158 to 162, 170 to 186, and 192 to 198; C_H: 119 to 127, 139 to 152, 154 to 159, 166 to 170, 172 to 193, and 198 to 204. From the direction cosines of the rotation axis, as determined by the program, the elbow angle was calculated using the formula: $\cos\ \theta = \cos\ \alpha_1\ \cos\ \alpha_2 + \cos\ \beta_1\ \cos\ \beta_2 + \cos\ \gamma_1\ \cos\ \gamma_2$. The programs Molscript (Kraulis, 1991) and Raster3D (Merritt & Murphy, 1994) were used in the Figure preparations. Atomic coordinates for both crystal forms I and II have been deposited at the Brookhaven Data Bank with the entry-codes 1HYX and 1HYY, respectively.

Determination of dissociation and inhibition constants for haptenic phosphonates

Dissociation constants were determined by fluorescence titration, with a Hitachi F-4000 spectrophotometer. The formation of hapten complexes of the Fab 6D9 was followed by measuring the tryptophan quenching upon the addition of increasing concentrations of the hapten. The fluorescence intensity was measured at 340 nm, using an excitation wavelength of 295 nm. To 2.0 ml of 0.03 μM Fab 6D9 in 50 mM

Hepes (pH 8.0) was added small aliquots of 10 μM hapten in the same buffer at 25°C, and the change (ΔF) of the flourescence was determined. The plots of $[L]_0/\Delta F$ *versus* $[L]_0$, where $[L]_0$ represents the total hapten concentration, provides the dissociation constant (K_d) as the intercept. The inhibition constant, K_i, was determined from the Dixon plots (Fujii *et al.*, 1995).

Acknowledgments

The major part of this project was realized during a stay of O.K. at the Protein Engineering Research Institute (PERI), Osaka. We thank our colleagues at PERI for many fruitful discussions. We acknowledge the Photon Factory, Tsukuba, for providing synchrotron radiation facilities. O.K. was supported by a grant from the European Communities S&T Fellowship Programme in Japan, No. CIPI30024.

References

Arevalo, J. H., Hassig, C. A., Stura, E. A., Sims, M. J., Taussig, M. J. & Wilson, I. A. (1994). Structural analysis of antibody specificity. detailed comparison of five fab′-steroid complexes. *J. Mol. Biol.* **241**, 663–690.

Bartlett, P. A. & Marlowe, C. K. (1987). Evaluation of intrinsic binding energy from a hydrogen bonding group in an enzyme inhibitor. *Science,* **235**, 569–571.

Bash, P. A., Singh, U. C., Brown, F. K., Langridge, R. & Kollman, P. A. (1987). Calculation of the relative change in binding free energy of a protein-inhibitor complex. *Science,* **235**, 574–576.

Branden, C. & Tooze, J. (1991). *Introduction to Protein Structure*, Garland Publishing, Inc., New York.

Brünger, A. T. (1990). Extension of molecular replacement: A new search strategy based on Patterson correlation refinement. *Acta. Crystallog. sect. A,* **46**, 46–57.

Brünger, A. T. (1992). *X-PLOR, Version 3.1, A System for X-ray Crystallography and NMR*, Yale University Press.

Burley, S. K. & Petsko, G. A. (1985). Aromatic-aromatic interaction: a machanism of proten structure stabilization. *Science,* **229**, 23–28.

Chacko, S., Silverton, E., Kam-Morgan, L., Smith-Gill, S., Cohen, G. & Davies, D. (1995). Structure of an antibody-lysozyme complex: Unexpected effect of a conservative mutation. *J. Mol. Biol.* **245**, 261–274.

Charbonnier, J. B., Carpenter, E., Gigant, B., Golinelli-Pimpaneau, B., Eshhar, Z., Green, B. S. & Knossow, M. (1995). Crystal structure of the complex of a catalytic antibody Fab fragment with a transition state analog: structural similarities in esterase-like catalytic antibodies. *Proc. Natl Acad. Sci. USA,* **92**, 11721–11725.

Charbonnier, J. B., Golinelli-Pimpaneau, B., Gigant, B., Tawfik, D. S., Chap, R., Schindler, D. G., Kim, S.-H., Green, B. S., Eshar, Z. & Knossow, M. (1997). Structural convergence in the active sites of a family of catalytic antibodies. *Science,* **275**, 1140–1142.

Deslongchamps, P. (1983). Esters and related functions. In *Stereoelectronic Effects in Organic Chemistry*, pp. 54–100, Pegamon Press, Oxford.

Fersht, A. (1985). Ensyme-substrate complementarity and use of binding energy in catalysis. In *Enzyme Structure and Mechanism*, 2nd edit., pp. 311–346, W. H. Freeman and Company, New York.

Fujii, I., Tanaka, F., Miyashita, H., Tanimura, R. & Kinoshita, K. (1995). Correlation between antigen-combining-site structures and functions within a panel of catalytic antibodies generated against a single transition state analog. *J. Am. Chem. Soc.* **117**, 6199–6209.

Golinelli-Pimpaneau, B., Gigant, B., Bizebard, T., Navaza, J., Saludjian, P., Zemel, R., Tawfik, D. S., Eshhar, Z., Green, B. S. & Knossow, M. (1994). Crystal stucture of a catalytic antibody Fab with esterase-like activity. *Structure,* **2**, 175–183.

Guddat, L. W., Shan, L., Anchin, J. M., Linthicum, D. S. & Edmundson, A. B. (1994). Local and transmitted conformational changes on complexation of an anti-sweetener Fab. *J. Mol. Biol.* **236**, 247–274.

Guo, J., Huang, W. & Scanlon, T. S. (1994). Kinetic and mechanistic characterization of an efficient hydrolytic antibody: evidence for the formation of an acyl intermediate. *J. Am. Chem. Soc.* **116**, 6062–6069.

Higashi, T. (1989). The processing of diffraction data taken on a screenless Weissenberg camera for macromolecular crystallography. *J. Appl. Crystallog.* **22**, 9–18.

Jones, T. A., Cowan, S., Zou, J.-Y. & Kjeldgaard, M. (1991). Improved methods for building protein models in electron density maps and the location of errors in these models. *Acta Crystallog. sect. A,* **47**, 110–119.

Kleywegt, G. J. & Jones, T. A. (1994). A super position. *ESF/CCP4 Newsletter,* **31**, 9–14.

Kraulis, P. J. (1991). MOLSCRIPT: a program to produce both detailed and schematic plots of protein structures. *J. Appl. Crystallog.* **24**, 946–950.

Kristensen, O., Miyashita, H., Vassylyev, D. G., Tanaka, F., Fujii, I. & Morikawa, K. (1995). Crystallization and preliminary X-ray analysis: transition state complex of a chloramphenicol prodrug specific catalytic antibody. *Protein Pep. Letters,* **1**, 252–255.

Laskowski, R. A., MacArthur, M. W., Moss, D. J. & Thornton, J. M. (1993). PROCHECK: a program to check the stereochemical quality of protein structures. *J. Appl. Crystallog.* **26**, 283–291.

Lerner, R. A. & Schultz, P. G. (1993). Antibody catalysis of difficult chemical transformations. *Acc. Chem. Res.* **26**, 391–395.

Lerner, R. A., Benkovic, S. J. & Schultz, P. G. (1991). At the crossroads of chemistry and immunology: catalytic antibodies. *Science,* **252**, 659–667.

MacBeath, G. & Hilvert, D. (1996). Hydrolytic antibodies: variations on a theme. *Chem. Biol.* **3**, 433–445.

McRee, D. E. (1992). A visual protein crystallographic software system for X11/Xview. *J. Mol. Graphics,* **10**, 44–46.

Merritt, E. A. & Murphy, M. E. P. (1994). Raster3D Version 2.0 – a program for photorealistic molecular graphics. *Acta. Crystallog. sect. D,* **50**, 869–873.

Miyashita, H., Karaki, Y., Kikuchi, M. & Fujii, I. (1993). Prodrug activation via catalytic antibodies. *Proc. Natl Acad. Sci. USA,* **90**, 5337–5340.

Miyashita, H., Hara, T., Tanimura, R., Tanaka, F., Kikuchi, M. & Fujii, I. (1994). A common ancestry for multiple catalytic antibodies generated against a single transition-state analog. *Proc. Natl Acad. Sci. USA,* **91**, 6045–6049.

Miyashita, H., Hara, T., Tanimura, R., Fukuyama, S., Cagnon, C., Kohara, A. & Fujii, I. (1997). Site-

directed mutagenesis of active site contact residues in a hydrolytic abzyme: evidence for an essential histidine involved in transition state stabilization. *J. Mol. Biol.* **267**, 1247–1257.

Otwinowski, Z. (1993). *Data Collection and Processing: Proceedings of the CCP4 Study Weekend, 29–30 January*. Daresbury Laboratory, Warrington WA4 4AD, UK.

Padlan, E. A. (1994). Anatomy of the antibody molecule. *Mol. Immunol.* **31**, 169–217.

Patten, P. A., Gray, N. S., Yang, P. L., Marks, C. B., Wedemayer, G. J., Boniface, J. J., Stevens, R. C. & Schultz, P. G. (1996). The immunological evolution of catalysis. *Science,* **271**, 1086–1091.

Schultz, P. G. & Lerner, R. A. (1995). From molecular diversity to catalysis: lessons from the immune system. *Science,* **269**, 1835–1842.

SERC (1979). *Collaborative Computing Project No. 4, A Suite of Programs for Protein Crystallography*, Daresbury Laboratory, Warrington WA4 4AD, UK.

Shokat, K. M. & Schultz, P. G. (1990). Catalytic antibodies. *Annu. Rev. Immunol.* **8**, 335–363.

Stanfield, R. L., Fieser, T. M., Lerner, R. A. & Wilson, I. A. (1990). Crystal structures of an antibody to a peptide and its complex with peptide antigen at 2. 8 Å. *Science,* **248**, 712–719.

Steigemann, W. (1974). Die Entwicklung und Anwendung von Rechen-programmen zur Strukturanalyse von Proteinen am Beispiel des Trypsin-Trypsininhibitor Komplexes, des freien Inhibitors und der L-Asparaginase. PhD, Technical University of Munich, Germany.

Stewart, J. D. & Benkovic, S. J. (1995). Transition-state stabilization as a measure of the efficiency of antibody catalysis. *Nature,* **375**, 388–391.

Tramontano, A., Janda, K. D. & Lerner, R. A. (1986). Catalytic antibodies. *Science,* **234**, 1566–1570.

Tronrud, D. E., Holden, H. M. & Matthews, B. W. (1987). Structures of two thermolysin-inhibitor complexes that differ by a single hydrogen bond. *Science,* **235**, 571–574.

Tulip, W. R., Varghese, J. N., Laver, W. G., Webster, R. G. & Colman, P. M. (1992). Refined crystal structure of the influenza virus N9 neuraminidase-NC41 Fab complex. *J. Mol. Biol.* **227**, 122–148.

Wang, B.-C. (1985). Resolution of phase ambiguity in macromolecular crystallography. *Methods Enzymol.* **115**, 90–112.

Wedemayer, G. J., Wang, L. H., Patten, P. A., Schultz, P. G. & Stevens, R. C. (1997). Crystal structures of the free and liganded form of an esterolytic catalytic antibody. *J. Mol. Biol.* **268**, 390–400.

Zhou, G. W., Guo, J., Huang, W., Fletterick, R. J. & Scanlan, T. S. (1994). Crystal structure of a catalytic antibody with a serine protease active site. *Science,* **265**, 1059–1064.

Edited by I. Wilson

(Received 8 December 1997; received in revised form 23 April 1998; accepted 11 May 1998)